Process Safety and Environmental Protection 184 (2024) 601–614

Contents lists available at ScienceDirect

Process Safety and Environmental Protection

journal homepage: www.journals.elsevier.com/process-safety-and-environmental-protection

Measurement of transient nanoparticle emissions of a municipal biomass incineration plant equipped with pulse-jet cleaned filters

P. Bächler [a,*], J. Meyer [a], R. Ligotski [b], P. Krug [b], A. Dittler [a]

[a] Institute of Mechanical Process Engineering and Mechanics, Karlsruhe Institute of Technology, Karlsruhe, Germany
[b] BWF Envirotec GmbH, Offingen Germany

ARTICLE INFO

Keywords:
Baghouse filter
Nanoparticles
Emission measurement
Gas cleaning
Pulse-jet cleaned filter
Biomass combustion

ABSTRACT

The nanoparticle emission of a biomass incineration plant for district heating was investigated during a field measurement campaign. Pulse-jet cleaned filters were used as the main waste-gas treatment technology for the plant, downstream of a multi-cyclone which served as a pre-separator for the coarser size spectrum of fly ash particles. These filters feature a characteristic transient emission behavior consisting of distinct emission peaks, lasting from several seconds to many minutes after filter regeneration. This transient behavior required the development of an adapted measurement setup and methodology when using a scanning mobility particle sizer (SMPS) for the determination of the size distribution. The concentration of particle size fractions (during both, SMPS scans and measurements with fixed classifier voltage) and the total concentration were measured simultaneously applying two condensation particle counters (CPC). The decay behavior of the emission peaks of certain size fractions (at fixed classifier voltage) and the total concentration are in good agreement, enabling post-processing of the SMPS scans, which are affected by the inlet concentration decay during measurement. The size distributions of the particle emission from filter bags made of needle-felt media (aged and newly installed) and of membrane filter medium with taped seams (newly installed) were obtained following the measurement methodology. The emission of the aged needle-felt and the membrane filter medium rapidly declined to zero, allowing only for a single scan for each regeneration event. The membrane filter medium shows the lowest emission at an average number concentration of approx. 13 #/cm^3 with a number-based median diameter $x_{50,0}$ of 70 – 80 nm. The results demonstrate the possible high number based separation efficiency (e.g. above 99.999 % for the membrane filter bag) of pulse-jet cleaned filters regarding particle sizes not properly represented by conventional gravimetrical measurements.

1. Introduction

Statutory limits for the particle emissions of industrial processes are typically based on a gravimetrically derived mass-based total concentration. E.g. the current BAT (best available techniques) reference document for common waste gas management and treatment systems in the chemical sector (WGC BREF) generally limits the total dust emission for fabric filters as the final waste-gas cleaning technology (for significant emission mass flows exceeding 50 g/h) at a mass-based concentration of 5 mg/m^3 (European Commission et al., 2023). The size of the emitted particles is typically not considered for emission monitoring while air quality limits for ambient air do take into account particle size, and e.g. the $PM_{2.5}$ or PM_{10} fraction is measured. Finer particle sizes are particularly harmful for human health and the environment (German National Academy of Sciences Leopoldina, 2019). Particles in the nanometer size region (e.g. ultra fine particles (UFP) with $x < 100$ nm) are known to be able to penetrate deeper into the lungs or even enter the bloodstream, increasing the risk of cardiovascular

Abbreviations: BAT, Best Available Techniques; EDX, Energy dispersive X-ray spectroscopy; SMPS, Scanning mobility particle sizer; DMA, Differential mobility analyzer; PSD, Particle size distribution; OPC, Optical particle counter; SEM, Scanning electron microscope; Cn,tot [#/cm^3], Total particle number concentration; Cn, fraction [#/cm^3], Particle number concentration of a certain particle size fraction; Cn,peak[#/cm^3], Number concentration at the maximum of the emission peak; Δp [Pa], Filter differential pressure; q_0x [nm^{-1}], Normalized number density distribution; $x_{50,0}$ [nm], Median particle diameter; x [nm], Particle diameter; Δx [nm], Interval width of a size fraction; x_{min} [nm], Lower limit of size distribution; x_{max} [nm], Upper limit of size distribution; f_i [-], Scaling factor for the individual density distributions; f* [-], Scaling factor for the mean density distribution; n [-], Number of samples.

* Corresponding author.
E-mail address: peter.baechler@kit.edu (P. Bächler).

https://doi.org/10.1016/j.psep.2024.02.013
Received 22 November 2023; Received in revised form 22 January 2024; Accepted 5 February 2024
Available online 8 February 2024

diseases, dementia and other diseases (Mishra and Sundaram, 2023; Ohlwein et al., 2019). Air pollution is a cause for premature deaths and the role of ultrafine particles regarding adverse health effects and the necessity for measurements is currently discussed regarding e.g. the revision of air quality standards like the EU Ambient Air Quality Directive (2008/50/EC) or WHO guidelines (European Commission, 2024; Soares et al., 2022; WHO global air quality guidelines, 2021). While the drive for lower particle concentrations exists in both cases regarding particle emissions from technical applications and ambient air quality, the role of industrial processes regarding nanoparticle emissions is not properly reflected in the current gravimetrical limits.

Baghouse filters remain one of the most important gas cleaning technologies for particle separation to this day and generally allow for low particle emission levels. The regeneration capabilities of the filters enable continuous operation even under higher dust loads (Schmidt, 1998, Klingel and Löffler, 1983; Leith and Ellenbecker, 1980). During filter operation, particles are separated primarily at the surface of the filter medium causing the formation of a dust cake with a near perfect separation efficiency (zero concentration) (Zhang, 2021). Particle penetration only occurs directly after filter regeneration (e.g. via pulse-jet) when the dust cake is removed. This leads to a characteristic transient emission behavior, where distinct particle emission peaks (or a decaying clean gas particle concentration) can be detected after each regeneration at the corresponding filter element before reaching a zero level (Bächler et al., 2020). The predominant penetration mechanism during this emission peak is “straight through” the filter medium so that surface treatment and filter media properties can lower particle emissions by enhancing and enabling the fast formation of dust cakes on the surface of the filter material (Binnig et al., 2009). Thus, the filter medium (among other process conditions like flow velocity, raw-gas concentration, regeneration intensity, etc.) has an effect on the height and concentration decay of particle emission peaks (Bächler et al., 2019). Typical surface treatments for filter media are e.g. lamination of a membrane on the upstream side, calendaring or singing of the upstream side (Cirqueira et al., 2017). Note that in real-world applications, leaks of the filter medium or the plenum plate, insufficient sealing, etc. may also contribute to the total dust emission and serve as a spatial emission hotspot in a filter house (Bach and Schmidt, 2007; Bächler et al., 2023a; 2022).

The wide application spectrum of cleanable fabric filters includes many processes where nanoparticles are part of the raw-gas aerosol and have to be separated from the dust-laden gas stream. Incineration processes, such as the combustion of waste, biomass or other solid fuels generate particles in the nanometer region and may also rely on pulse-jet cleaned filters for gas cleaning (Schott et al., 2022). In some cases, the protection of the filter medium with a coarser pre-coat dust cake is necessary in order to avoid clogging of the filter medium and exceedingly high differential pressures (Khirouni et al., 2020, Schiller and Schmid, 2015).

The combustion of “renewable” wood biomass is still gaining relevance in the context of rising energy costs and climate change. Small scale furnaces may generate heat for individual homes, however dedicated gas cleaning technologies are only rarely applied and exhaust fumes are emitted into the surrounding neighborhoods contributing to the air pollution in residential areas (Thieringer et al., 2022; Bari et al., 2010). Municipal incineration plants may provide district heating networks for larger amounts of buildings and require dedicated gas-cleaning technologies due to their larger scale (Eriksson et al., 2007; Monsberger et al., 2023; Soltero et al., 2023). In a recent publication, Steiner & Lanzerstorfer report mass based dust emissions from biomass incineration processes, where gas cleaning applying cleanable fabric filters could well comply with the new BAT-limits. However, uncertainties of (gravimetrical) measurement devices under these low gravimetric concentrations can become an issue (Steiner and Lanzerstorfer, 2023). The actual emission of nanoparticles into the environment from plants equipped with fabric filters has not been subject of research and due to the small particle size, mass resolved limits may not always comprise and restrict the actual (nano-) particle emission (Zhang et al., 2023).

Due to the transient nature of particle emissions in baghouse filters, correct online particle measurement in the nanometer region is a challenge. Field-measurement-suitable optical particle counters based on the detection of scattered light on a single particle have a lower detection limit of approximately 200 – 300 nm so that the detection of nanoparticles in the range of $x < 100$ nm is not possible. In a recent study, an engine exhaust particle sizer (EEPS) was tested for the measurement of the characteristic emission behavior of pulse-jet cleaned filters on a lab-scale. The main drawback of the device was a minimum concentration threshold for smaller particle sizes that prevents measurement of a zero emission level (with an established dust cake) and which may also be too high to correctly detect emission peaks, especially when dealing with efficient (membrane) filter media (Bächler et al., 2022a). State of the art measurement technology for low-concentration submicron aerosols is the application of scanning mobility particle sizers (SMPS) consisting of a differential mobility analyzer (DMA) in combination with a condensation particle counter (CPC). Particles of a defined size may pass the DMA based on their electrical mobility and the applied voltage of the DMA and are subsequently detected at the CPC. Varying the voltage enables passage of different size classes and thus “scanning” of a particle size distribution (PSD). Under ideal measurement conditions for SMPS systems, the particle concentrations of the corresponding size fractions remain constant for the entire scanning procedure. Under constant conditions, several scans may be performed back to back in order to determine representative average size distributions (Kaminski et al., 2013). Since the determination of a complete PSD requires a certain scanning time of the SMPS system, the determination of size distributions of transient concentration events, as they occur in the form of emission peaks in pulse-jet cleaned filters, pose a significant measurement challenge. Schiller & Schmid reported grade efficiencies from SMPS measurements from a baghouse filter in a similar application, however the measurement procedure was not further specified. In their publications, average distributions not explicitly considering the transient behavior were presented where the grade efficiency in the nanometer region approaches unity (complete separation) (Schiller and Schmid, 2013, 2014, 2015). Simon et al. reported the fractional efficiency of filter media for pulse-jet cleaned filters measured (among other instruments) with an SMPS system. However, flat sheet media samples were used applying a test aerosol and not during real filter operation (Simon et al., 2014). Several other publications exist on the topic of measurements at industrial baghouse filters or on a pilot-plant scale (e.g. Bächler et al., 2023b; Ergüdenler et al., 1997; Rogoziński, 2018; Saleem et al., 2012; Simon et al., 2010, 2014; Tsai et al., 2000), however, to the authors’ knowledge, the measurement of transient nanoparticle emissions has not been covered.

This investigation presents the result of a measurement campaign at a municipal biomass incineration plant equipped with pulse-jet cleaned filters as waste-gas cleaning technology in a German town. In order to measure the nanoparticle emission of the pulse-jet cleaned filters, a complex measurement methodology and a corresponding measurement setup was developed for the correct determination of particle size distributions despite the transient nature of the particle emission peaks. The particle size distributions and the number concentrations of the particle emission for three different filter bags made of different media and with two different sealing concepts were determined.

2. Experimental set-up, procedures and materials

2.1. Municipal biomass incineration plant

The measurements were performed in a municipal biomass incineration plant in the German town of “Günzburg”. The biomass incineration plant supplies the surrounding districts with heat at a power output of

max. 0.85 MW. Regarding German legislature, the power plant is classified as small and medium firing installation according to the 1st federal emission control ordinance (1. BImSchV). The fuel for the combustion process consists of wood (mainly offcuts / wood chips from the surrounding region). The measurement campaign lasted several days, whereby the results presented in this study were obtained during a three-day period of actual measurements. The exhaust gas from the combustion is treated with a multicyclone as pre-separator and pulse-jet cleaned filters before being released into the environment at the stack. A flow-sheet of the exhaust gas treatment and an overview of the pulse-jet cleaned filter is displayed in Fig. 1.

The pulse-jet cleaned filter is operated at a temperature of approx. 180°C. If a temperature of 230°C is reached (what may only occur during special high-load scenarios), the filter is bypassed and exhaust gas after the multicyclone is led directly to the stack. The volume flow is specified between 3900 and 4400 $m^3_{i.N.}$/h dependent on the temperature. While there are daily fluctuations of the process parameters for the filter (e.g. inlet temperature 160 – 220°C, differential pressure 1.5–8 mbar and fan power 20 – 50% of maximum capacity), the limited data availability does not allow for conclusions on the impact of process parameters of the incineration plant on particle emissions. The clean gas side of the baghouse is divided into two separate chambers of uniform size. A total of 120 filter bags (total filter area of approx. 140 m^2) is arranged in 10 rows of 12 bags each. The cleaning strategy was a "row-by-row" cleaning algorithm, progressing to the nearest neighboring row. Filter regeneration is time controlled, so that one row of filter bags is regenerated by jet-pulse cleaning after a fixed time interval. The time interval depends on the current differential pressure level as summarized in Table 1. During the measurement campaign, a time interval of 8 min between the individual regenerations of neighboring rows was preset for the vast majority of cases. Thus, a complete filtration cycle (regeneration of the complete series of ten rows within the two chambers) usually takes 80 min.

Probes at several measurement positions were installed beforehand. A picture displaying the aerosol sampling from the outlet of an individual filter element to the measurement setup and a more detailed description of the measurement procedure can be found in the supplementary information (figure SI2). Exploiting the time-controlled regeneration scheme enabled the consecutive measurement of particle emissions from filter bags in different rows. The emission declined to a zero level before the consecutive regeneration so that switching of the sampled filter element was possible before the consecutive regeneration in the majority of cases. Manually switching the sampled filter element helped reduce overall measurement times, which was critical due to limited access to the filter house.

Table 1
Time interval between filter regenerations.

Differential pressure threshold	Time interval between regenerations of individual rows
$\Delta p < 910$ Pa	8 min
910 Pa $< \Delta p <$ 1200 Pa	1.5 min
1200 Pa $< \Delta p$	1 min

The majority of installed filter elements (with the exception of two rows and two individual bags – refer to supplementary information figure SI3) were needle-felt filter bags (no sealing of the seams) installed during the last maintenance of the baghouse prior to the current heating season (2022/23). At the time of the measurements, the filters have been operated for approx. 5 months, so that, despite the relatively low filter age, no start-up effects are to be expected. Two rows in the corresponding filter chamber were equipped with filter bags made from membrane filter media. The seams of the membrane filter bags were sealed with PTFE tape sealing in order to avoid emission contributions from stitching holes (Lacerda et al., 2022). During the last maintenance, two single filter bags were not replaced, but have been left from the previous batch of installed filter bags (aged needle felt; lifetime: approx. 15.5 years seasonal operation of approx. 7–8 months per year). The aged and newly-installed needle-felt filter bags have slightly different properties in their original state but are very much comparable. The newly-installed filter bags are made of a current version of the PTFE needle-felt. An overview of the measurement positions within the baghouse can be found in the supplementary information (figure SI3). This setup enables the comparison between an aged and a newly installed needle-felt filter bag and newly installed membrane filter bags. Key properties of the filter media are summarized in Table 2. Additionally, an analysis of the used filter bags was performed following the measurement campaign (after heating season 2022/23). Filter samples were analyzed regarding area weight and permeability under different conditions (as received from the plant, regenerated and laundered). The filter bags were manufactured by BWF Tec GmbH & Co. KG, BWF Envirotec.

Flow measurements via Prandtl probes showed low flow velocities of approx. 0.4 – 0.7 m/s which are in the range of the lower detection limit of the testing probes. While there may be a spatial flow profile, the overall flow velocities are very low compared to other studies, where spatial differences regarding air flow and permeability through filter elements were investigated (Simon et al., 2010). The effect of different air permeabilities (compare Table 2) and potential spatial flow profiles

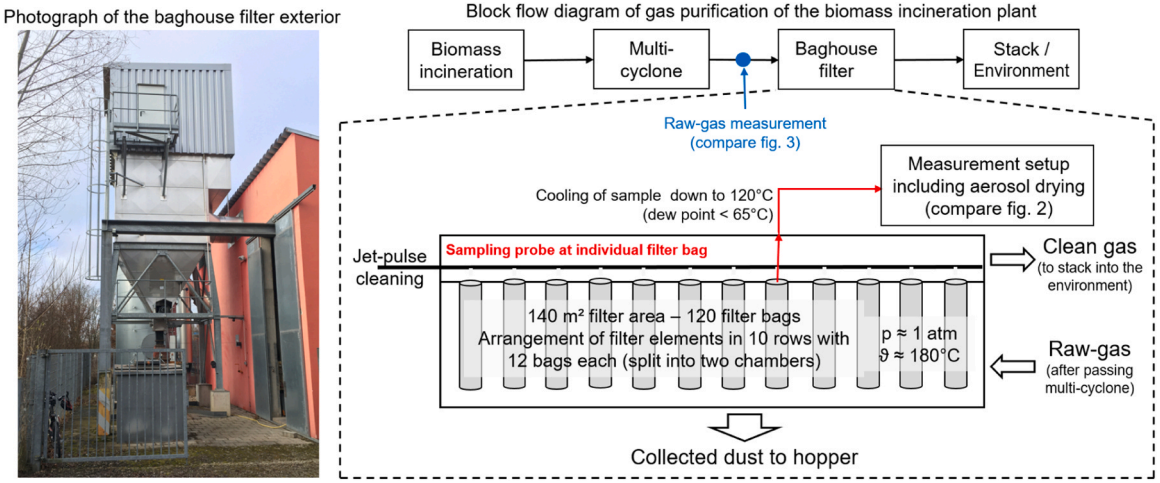

Fig. 1. Photograph of the exterior of the filter house (left) and block flow diagram of the waste gas treatment as well as schematic of the pulse-jet cleaned filter of the municipal biomass incineration plant (right).

Table 2
Overview of filter media characteristics.

Filter Medium	Aged needle-felt filter medium	Membrane filter medium	Needle-felt filter medium
Operating time	≈ 110–125 months (assuming an average annual operating time of 7–8 months)	≈ 5 months	≈ 5 months
Material	PTFE	PTFE	PTFE
Area weight of factory-new medium / gm^{-2}	700	750	700
Area weight – analysis of used bag/ gm^{-2}	As received: 837 Jet-pulse cleaned: 792 Laundered: 721	As received: 798 Jet-pulse cleaned: 787 Laundered: 775	As received: 837 Jet-pulse cleaned: 778 Laundered: 737
Thickness of factory-new medium / mm	1.4	1.2	1.3
Permeability (200 Pa) of factory-new medium / $Ldm^{-2}min^{-1}$	120 (−17/+30)	30 (±15)	100 (−50/+20)
Permeability (200 Pa) of used bag / $Ldm^{-2}min^{-1}$	As received: 13 Jet-pulse cleaned: 39 Laundered: 103	As received: 10 Jet-pulse cleaned: 13 Laundered: 19	As received: 11 Jet-pulse cleaned: 26 Laundered: 48
Remarks:	Heat-set, calendered upstream side, PTFE fiber impregnation, micropores (due to fiber size)	Heat-set, ePTFE membrane; Sealed longitudinal and cross seams of the filter bag	Heat-set, calendered upstream side, PTFE fiber impregnation, micropores (due to fiber size)

were not considered on the measured concentrations in the investigation.

The amount of corrosive gases (e.g. HCl and SO_2) is very low, so that falling below the dew-point of the acids or corrosive damage to the equipment can be ruled out. However, the raw-gas has a relatively high water vapor content of approx. 25 Vol.-%, so that aerosol drying is necessary to avoid condensation and significant particle losses in the sampling and measurement line when falling below the dew point. According to the plant specification, the dew-point of the raw-gas aerosol is approx. 65°C. Further information on the raw-gas aerosol can be found in Section 2.3.

2.2. Measurement setup

As the characteristic emission behavior of pulse-jet cleaned filters consists of transient events that may only be detectable for several minutes (or even seconds) before declining to a zero level, an elaborate measurement setup and procedure was developed. Additionally, the hot exhaust gas posed several challenges, mainly due to the high water content from the combustion of woody and partly damp biomass (wood chips). The (sample) temperature must not fall below the dew point of 65°C (before aerosol drying).

Fig. 2 displays a flow-sheet of the measurement setup highlighting the main components. A photograph of the setup can be accessed in the supplementary information (figure SI1).

The samples were taken at the outlet of each filter element as described in Section 2.1. and in the supplementary information, and transferred into the measurement setup via conductive PTFE tubing installed in the head space of the filter house. The internal pump of a PROMO®2000 H from the manufacturer PALAS® drew a total sample flow of approx. 5 L/min. A heating tube served as electric trace heating system to avoid cooling of the sample flow below the dew-point and subsequent condensation in the transfer line between filter house and measurement system. The total sample flow then passed a heated WELAS®2300 H sensor at a temperature of 110°C. Note that the detected particle sizes were mainly below the detection limit of the PALAS® OPC, thus these OPC measurements are not relevant for the investigation (apart of proving the non-existence of a significant supermicron size fraction). Exemplary data from the scattered light-based detection can be accessed in the supplementary information (figure SI5). Afterwards, the aerosol flow was split into an excess flow and a sample flow for nanoparticle measurement. The excess flow was led outside of the filter house for condensation in a condensation vessel and merged with the rest of the sample flow further down the line. The sample flow itself passed a drying section consisting of two heated Nafion® dryers in series. The exact drying parameters can be accessed in the supplementary information (figure SI4) and the conditions are put into context with literature (Hermansson et al., 2011). After passing the drying section, the humidity of the sample was measured and the sample flow was split in two parts, whereby one part was directly entering a CPC in order to monitor the total particle number concentration (CPC 3775) and the other part of the sample flow was led to an SMPS system (TSI® Electrostatic Classifier Model 3082 with Advanced Aerosol Neutralizer 3088, Long DMA 3081A00 and CPC 3756).

The total particle number concentration $C_{n,tot}$ could be monitored with a high temporal resolution of 1 Hz. Simultaneously, size resolved information and classified particle number concentrations $C_{n,fraction}$ could be drawn from the SMPS system either in the form of distinct particle sizes (constant voltage at DMA) or in the form of SMPS scans (variation of DMA voltage over a certain time period). Both measurement modes of the SMPS system were used in the investigations to determine the emission PSD for the different filter media. The sheath flow of the DMA (when the CPC 3756 operated in the high flow mode) was set to 7.5 L/min. Scanning time was adjusted for each filter medium (compare Section 3.2. & 3.3.) and multiple charge correction and diffusion correction were considered in the evaluation software.

After passing the two CPCs, the sample flows and the excess flow were merged and pass HEPA and activated carbon filters for the protection of the PROMO®2000 system.

Particle losses due to the measurement setup were taken into account (compare Section 4.2) and a rudimentary transfer function could be

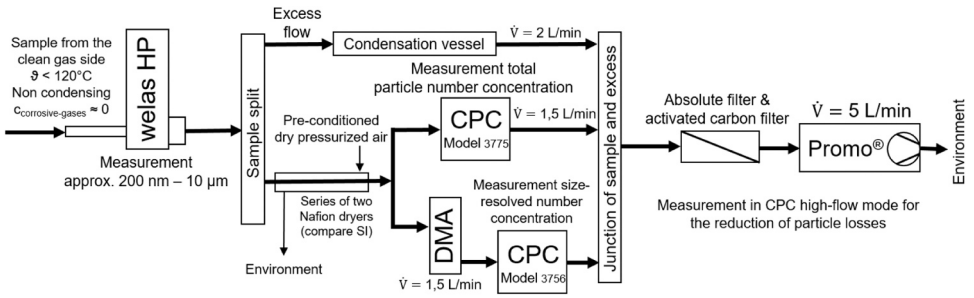

Fig. 2. Flow sheet of the measurement setup.

derived from measurements of the ambient aerosol (refer to supplementary information – figure SI10). The losses amount to approx. 52 % across all size fractions. Both CPCs were operated in the high flow mode (1.5 L/min sample flow for each CPC) during the filter emission measurements to minimize particle losses.

2.3. Characterization of the raw-gas aerosol

For better context regarding the separation efficiency of the pulse-jet cleaned filters, the raw-gas particle size distribution was measured and SEM / EDX analysis was performed. Samples from the raw-gas side could be accessed via a sample tube in a sealing plate, which was installed at one specific opening in the tube sheet instead of a filter bag (supplementary information – figure SI3). For the SEM analysis, two samples were taken. One sample was drawn through the measurement setup (dried and cooled down aerosol) and particles were separated on a Nucleopore® filter before the SMPS and CPC systems. Another sample was analyzed from a sample for gravimetrical concentration measurement (sampling on a micro-glassfiber filter connected directly to the trace-heated line after the filter house, not dried, hot aerosol). Regarding the determination of the raw-gas size distribution, contrary to the other measurements, the CPCs had to be operated in the "low flow mode" (sample flow of 0.3 L/min for each CPC), as the number concentration in the high flow mode was above the specifications of the CPCs and the measurements were affected by coincidence errors. Fig. 3 shows the average particle size distribution $q_0(x)$ (compare Eq. 3.1) of the raw-gas aerosol across a total of 37 scans. The total number concentration detected with the CPC 3775 was mostly above the measurement limit of 10^7 #/cm^3.

Only one measurement of the raw-gas aerosol was performed during the measurement campaign. Therefore, the determined PSD in Fig. 3 serves as a general fingerprint and fluctuations of the raw-gas may occur. The majority of particles are below the detection limit of the scattered light-based OPC and SMPS measurements are indeed necessary to capture the nanoparticle emission. The mode of the distribution is located at approx. 120 nm and the lower end of the size distribution is located at a particle size of approx. 30 nm (neglecting the artefacts at the lower end of the scanning size range, originating from quick repetition of subsequent scans). The size distribution corresponds well to the particle sizes found in the SEM analysis. Additionally, the detected particle sizes are comparable to results from other investigations found in literature (e.g. Helsper et al., 1980; Hueglin et al., 1997; Johansson et al., 2003; Obaidullah et al., 2012; Schiller and Schmid, 2015; Xie et al., 2007).

A gravimetric raw-gas measurement (sampling period of 40 min) yielded mass concentrations of the dry raw-gas of approx. 60 mg/m^3. This value also serves as a general fingerprint as a more exact quantification was not possible due to time constraints and fluctuations of process conditions and heat demand of the surrounding district may influence the raw-gas concentration.

An EDX analysis (Table 3) gives an indication on the chemical composition of the particles. Mainly potassium and calcium salts/oxides as well as sulphur components and carbon residues could be identified.

3. Measurement methodology for the determination of size distributions from transient particle emission peaks

Chapter 3 presents the methodology for the correct determination of particle size distributions from the transient concentration behavior typical for pulse-jet cleaned filters. Though chapter 3 stands separate from the results section, many exemplary measurement results are shown to illustrate the methodology.

Chapter 4 presents the final results and a comparison between the different filter media in the form of average and corrected particle size distributions according to the methodology introduced in chapter 3. Regarding particle size distributions, number density distributions $q_0(x)$ serve as the basis for comparison (normalized distribution – no impact of concentration), whereby x is the particle diameter, respectively the mean particle diameter of the corresponding size class. The density distribution can be calculated from SMPS data and the measured particle concentrations $C_{n,fraction}$ and $C_{n,tot}$ as well as the corresponding size fraction with the interval width Δx according to Eq. 3.1.

$$q_0(x) = \frac{C_{n,fraction}}{C_{n,tot} \bullet \Delta x} \tag{3.1}$$

3.1. Overall transient emission behavior of the different filter bags

The particle emission behavior of pulse-jet cleaned filters has been part of many previous investigations in literature (1998; Simon et al., 2014; Zhang, 20210). Shape and decaying time of the emission peak depend among many factors on the type of filter medium and the raw-gas concentration. Investigations in a small scale baghouse filter and filter test rigs applying scattered light-based aerosol spectrometers

Table 3
Chemical composition of particles from EDX analysis.

Element	Mass fraction / %
Carbon	21.342
Oxygen	29.504
Sodium	0.422
Magnesium	1.134
Silicon	0.158
Phosphor	1.404
Sulphur	7.502
Chlor	1.952
Potassium	19.974
Calcium	16.476
Iron	0.132

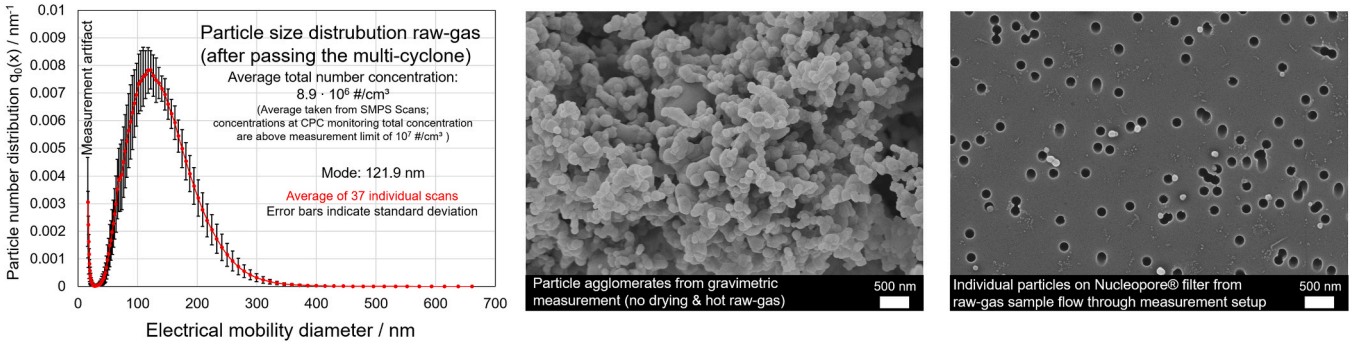

Fig. 3. PSD of the raw-gas aerosol (average of 37 subsequent scans of 90 s each – process conditions during the scan period: temperature between 170 and 190°C and differential pressure of approx. 3 mbar) (left) and SEM images (middle and right).

showed the differences between various types of filter media. Membrane filter media had emission peaks declining over very short time durations of several seconds while conventional needle-felt filter media had longer decay periods up to several minutes (Bächler et al., 2019, 2020, 2022b).

A similar behavior could be observed in the municipal biomass incineration plant. Fig. 4 shows exemplary data of particle emission peaks regarding the total particle concentration $C_{n,tot}$ from measurements over individual filter regeneration events. The time axis was aligned to set the maximum of the particle concentration peak at t = 0 for better comparison. The jet-pulse occurred approximately 9–10 s before the detection of the initial counting events and the sharp increase of the emission peak (residence time of CPC detector and sample line).

According to Fig. 4, three distinct types of behavior of the particle emission can be identified. The concentration measured from the aged needle-felt filter bag declines relatively quickly over the course of about 60–90 s and represents an intermediate concentration level. The emission of the membrane filter bag almost immediately (within 15–20 s) declines to a zero level and has the lowest emission level due to a negligible phase of depth filtration and a fast transition to cake formation on the membrane surface of the filter bag. The newly installed needle-felt has the highest emission and declines over the course of several minutes. Note that Fig. 4 only shows a relatively short time duration after the regeneration. Consequently, the total time interval until the emission of newly installed needle-felt filter bag reaches a zero level cannot be derived from the diagram in Fig. 4. Results over longer time periods for the decay of the particle emission for the newly-installed needle-felt can be found in the supplementary information (figure SI9). There have been cases, where the newly installed needle-felt declined (almost) over the total course of a complete filtration cycle (80 min). Additionally, the regeneration of neighboring rows of filter elements could be detected in the form of a related increase in dust emission for the newly-installed needle felt. This behavior corresponds to previous laboratory experiments regarding the spatial emission behavior of baghouse filters (Bächler et al., 2020, 2022b). Regarding the emission mechanisms, direct penetration is the predominant mechanism for the needle-felt filter media due to the long decay period. For the membrane filter medium, due to the short decay duration and low peak emission levels, entrainment of dust contaminations from surfaces on the clean-gas side may also affect the emission signal in addition to direct penetration. However, prior to the measurements during the installation of the sampling probes on the clean gas side, no visible dust contamination was identified on the clean gas-side. Thus, the predominant source of the emission cannot be designated with absolute certainty for the membrane filter element. The contribution of leaks to the particle emission can be ruled out due to the decline of the particle emission to a zero level, usually long before the end of the filtration cycle.

The transient emission behavior poses several challenges regarding the determination of the particle size distribution applying SMPS scans. The detected concentrations at the CPC after passing the DMA are affected by the concentration decay at the inlet of the DMA. For the newly installed needle-felt, the error is expected to be relatively small due to the comparably slow decline of the concentration. Here, averaging of multiple scans is possible in order to determine the particle size distribution from individual measurements after a single filter regeneration. For the aged needle-felt and more so for the membrane filter medium, the concentration decline happens so quickly that only a single scan is (barely) possible and the decay during this scan has to be considered when determining the size distribution.

The simultaneous concentration measurement of $C_{n,tot}$ and $C_{n,fraction}$ using two CPCs enables the correction of initial particle size distributions from SMPS scans assuming that the concentration decay of individual size classes is similar among all size fractions and does not change with increasing cake formation and declining particle concentration. To verify this assumption, a range of measurements was performed using the DMA as a classifier applying a constant voltage in order to obtain temporally resolved concentration curves (emission peaks) for certain distinct particle sizes and compare these to the decay of the total concentration. Fig. 5 illustrates the relative concentration decay of a specific size class ($x_{fraction}$ – red) and the total concentration (black). The total concentration $C_{n,tot}$ and the concentration of the size classified sample passing the DMA $C_{n,fraction}$ are normalized to the maximum concentration at the emission peak $C_{n,peak}$ and plotted as a function of time. The peaks have been aligned at the maximum of the emission peak (different residence time of the two sample flows within the measurement setup) for better comparison. The time until the first particles reach the detector of the corresponding CPC is 9–10 s for the total concentration and 16–17 s for the particle fraction for each filter element. The time until the maximum of the emission peak is reached varies dependent on the type of filter element. Shifting the time basis of the peaks to the corresponding maximum enables direct comparability of the decaying behavior.

While there are fluctuations regarding the maximum total concentrations $C_{n,peak}$ for each medium, different emission levels can already be identified. Note that the overall concentration curve of the emission for the membrane filter bag is only subject to minor fluctuations compared to the needle-felt filter bags and the behavior is very reproducible. The respective maxima of size-classified concentrations give indications on prevalent particle sizes and their frequency of occurrence within the emission PSD.

If the relative concentration decay for the size classified sample and the total concentration is similar, a correction of the detected concentrations during the SMPS scan, based on the total concentration curve is valid. The decay behavior of the emission peaks for the total concentration and for the respective simultaneously detected size class is in good agreement for all samples. Smaller deviations exist for particle

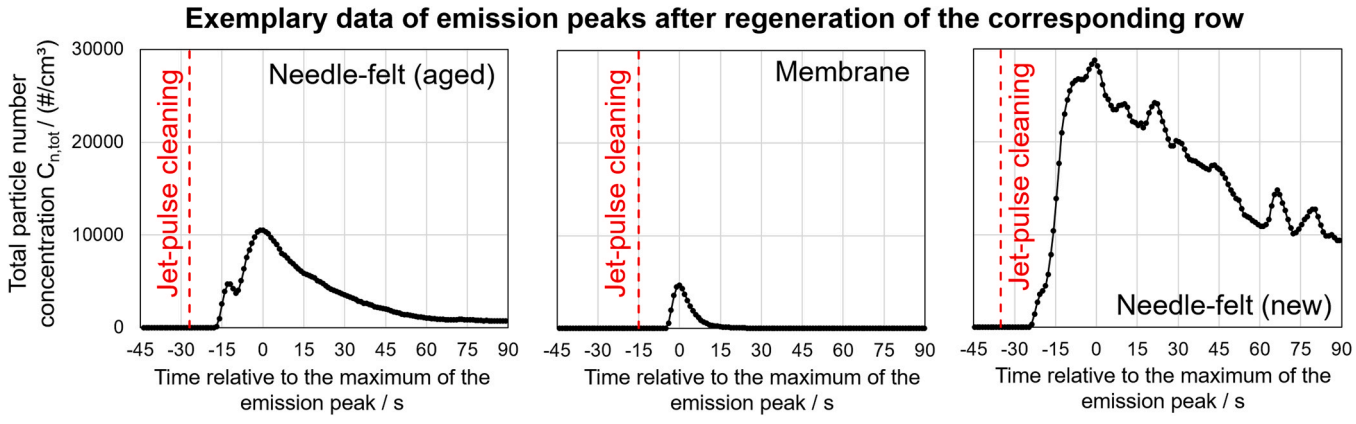

Fig. 4. Total particle concentration of the emission for the different filter elements after filter regeneration.

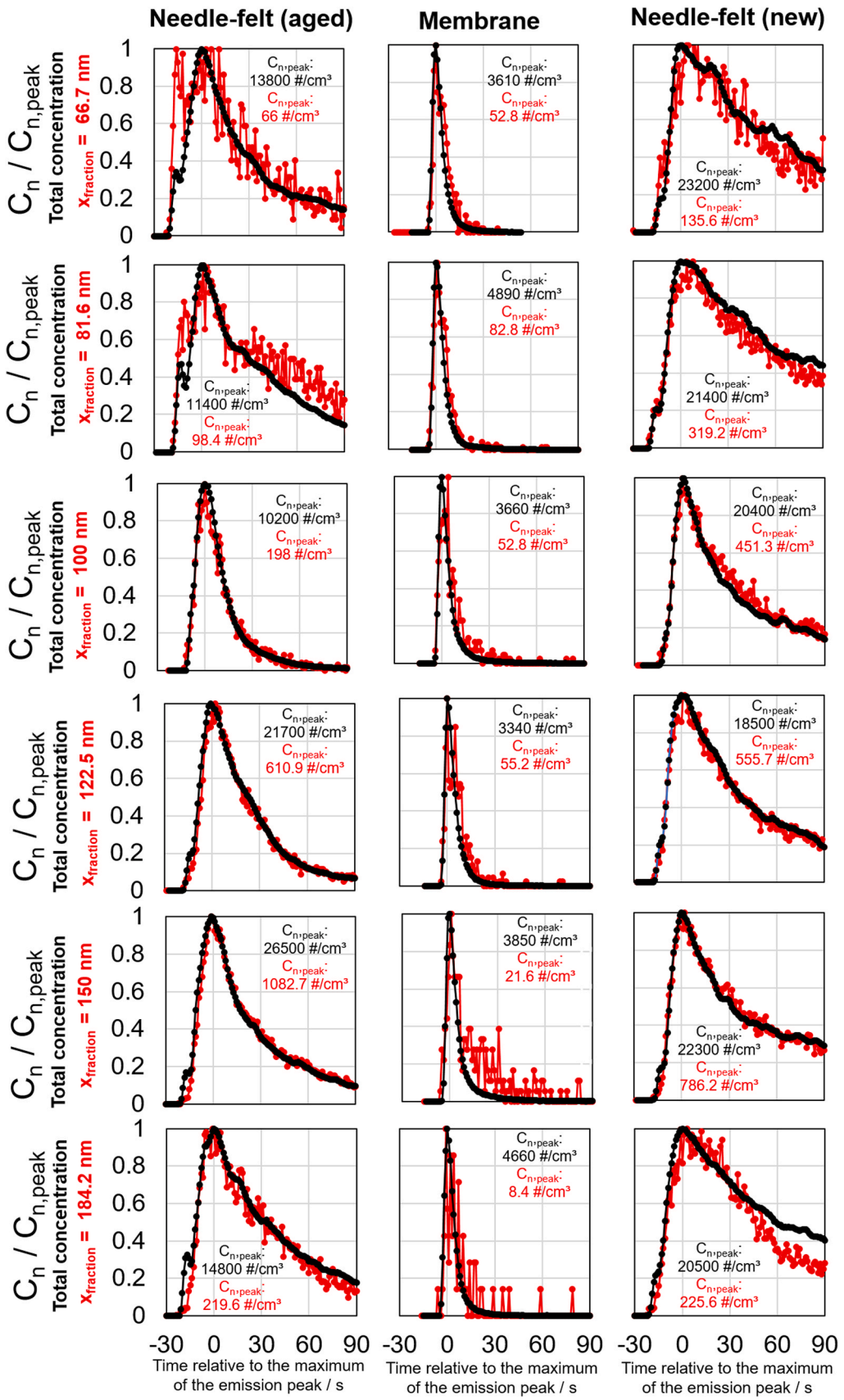

Fig. 5. Comparison of the normalized concentration decay of the total particle concentration $C_{n,tot}$ (black) and classified particle concentration $C_{n,fraction}$ of a single size class $x_{fraction}$ (red) for the different filter bags after filter regeneration. Note: each row of diagrams is derived from a different filtration cycle.

sizes close to the upper and lower end of the particle size distribution, where the number of counting events of the classified sample is very low (e.g. 66.7 nm and 184.2 nm measurements for the needle-felts).

Summarizing, the concentration decay of the tested size classes is independent of size and corresponds to the decaying behavior of the total concentration. Therefore, the relative decrease of particle concentration is similar and can be considered for SMPS measurements, where the detected particle size varies over the course of a scan. The scan properties (e.g. scan duration) have to be individually adjusted for each of the three different sample filter bags. While simple continuous scanning is possible for the new needle-felt filter bag with a relatively slow concentration decay, the measurements for the aged needle-felt filter bag and the membrane filter bag are likely to be affected by a concentration decay during SMPS scans, and thus, must be corrected.

3.2. Adaption of SMPS scan procedure and correction of scan data due to the transient emission behavior

For the correct execution of an SMPS scan in the field measurement, a thorough knowledge of the mean residence time/residence time behavior of the sample flow in the different sections of the measurement line is of paramount importance. This is one of the reasons why the investigations in Section 3.1. regarding the continuous concentration measurement of certain size classes at a constant DMA voltage and the corresponding decaying behavior were vital to the success of the measurements (Fig. 5). After filter regeneration, dust may penetrate the filter medium and a sample flow is drawn into the measurement setup. The regeneration itself occurred every 8 min and could be identified precisely on-site by the acoustic signal of the released jet-pulse. The time delay from the regeneration / acoustic signal until particles are finally detected at each CPC has to be characterized in order to identify a suitable point in time for the manual trigger to start the SMPS scan. The difference in runtime correction for both CPCs also has to be considered to correctly allocate the concentrations measured at each individual CPC (longer residence time for the aerosol flow passing the DMA and differences in CPC layout). The time until the first non-zero concentrations were detected was similar for all filter bags at the individual CPC, and thus, this time delay was used as the respective (minimum) runtime for each CPC. However, the time until the peak concentration was reached was different for each filter medium, depending on the details of flow reversal, cake release and redispersion during the regeneration. This is also reflected in Fig. 4 and Fig. 5 where the time axes are shifted accordingly to align at the respective peak of the transient particle concentration (local zero of time axes). Ideally, the beginning of a scan is triggered close to (or at) the concentration peak arriving at the inlet of the DMA. Delays of the computer control have to be considered regarding the manual starting trigger. Fig. 6 shows raw-data for two consecutive scans of the sample taken after regeneration of the aged needle-felt filter bag to demonstrate the behavior of total concentration $C_{n,tot}$ and particle size distribution as obtained by the SMPS system $dC_n/dlog(x)$ during a scan.

The concentration decay is directly visible in the concentration level of the two consecutive scans. Scan 2 is triggered at a lower concentration than scan 1, when the concentration has already decreased significantly. In the example displayed in Fig. 6, a third scan would yield only singular counting events. While the calculation of a normalized number density distribution $q_0(x)$ would create comparability between the PSDs obtained by the scans, the data would still be affected by the decaying behavior of the particle concentration. The relevance of the concentration decay for the membrane filter bag is even higher: since a zero level is reached after approx. 15 – 20 s, this requires much shorter scan durations compared to the needle-felt filter bags and allows for only one short scan per regeneration event.

The correct allocation of the point in time of the starting trigger for the scan enables the correction of the corresponding size classes based on the evolution of the total concentration. The procedure is illustrated in Fig. 7. The DMA voltage increases with time during a scan (upscan) so that particles with increasing size pass the DMA. Considering a certain scan duration, each size class i can be allocated to a corresponding point in time of detection t_i and thus, a momentary value of the total concentration $C_{n,tot}(t_i)$. Assuming uniform concentration decay of all size classes (compare Fig. 5), the relative concentration decay can be

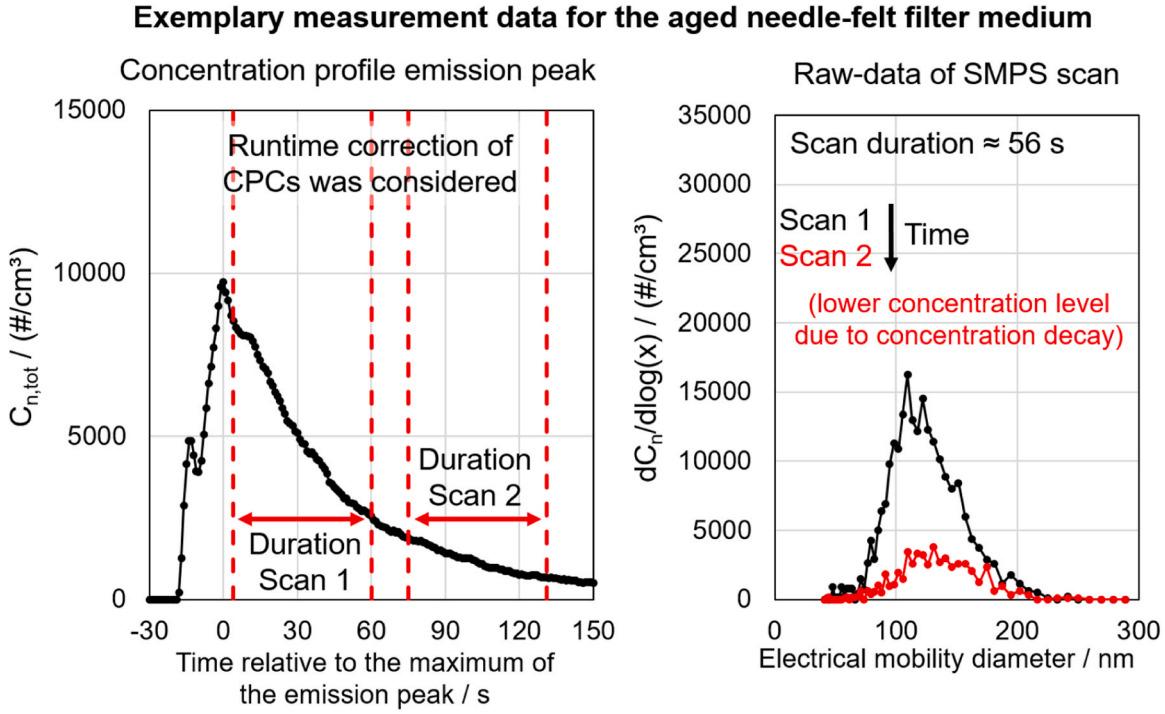

Fig. 6. Particle concentration profile (left) of the total concentration and measured particle size distribution (right) for two consecutive SMPS scans for the aged needle-felt filter bag (beginning of the first scan shortly after the maximum peak concentration).

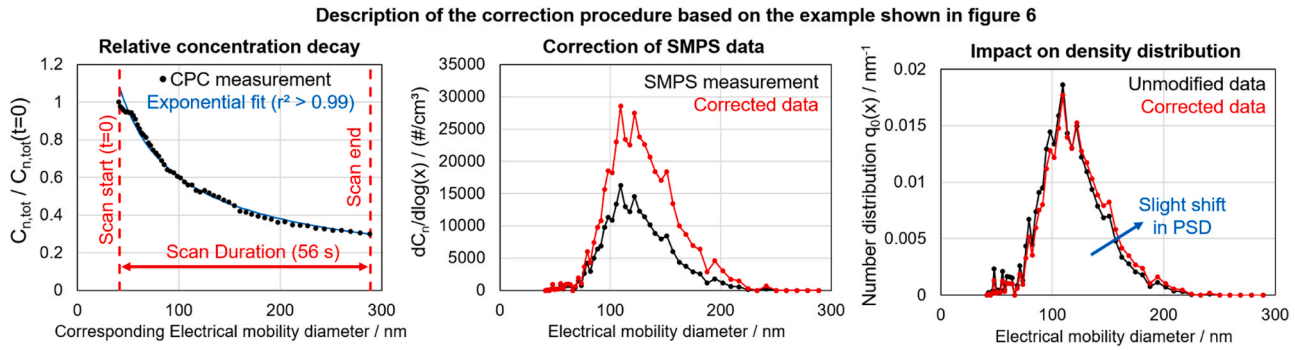

Fig. 7. Relative concentration decay (left) for the correction of the concentration in the individual size classes (middle) and the corresponding normalized density distribution (right).

calculated by the ratio of $C_{n,tot}(t_i)$ related to $C_{n,tot}(t=0)$ at the start of the scan. The relative concentration decay can subsequently be used to correct the concentration of the corresponding size classes (multiplication by the factor $C_{n,tot}(t=0)/C_{n,tot}(t_i)$). Note that in the example shown in Fig. 7, the relevant part of the size distribution (green) is measured in approx. 35 s, as sizes below 66.1 nm and above 224.7 nm are not relevant for the distribution (negligible concentrations – measured / verified experimentally). During this time, the relative concentration decays from 0.8 to 0.35 (≈ halving of concentration in the relevant region). Larger size-classes are more affected by the correction what slightly shifts the particle size distribution. The concentrations at the lower end of the adjusted size range for the SMPS scan are comparatively low. The correction does not have a large impact on these particle sizes as they occur close to the peak / start of the scan. Due to the moderate decay in the relevant size classes, the impact of the correction on the normalized density distribution is not as significant, especially around the peak of the size distribution.

While the impact of the correction on the normalized density distribution is only of minor significance in this example for the aged needle-felt filter bag, it will become increasingly relevant for quicker concentration decays. In general, the overall accuracy of the measurement is improved by the correction and the procedure had to be undergone in order to characterize the impact of the transient concentration behavior typical for pulse-jet cleaned filters. For the membrane filter bag, additional post-processing is required regarding the obtained measurement data due to the fast concentration decay and short scan durations (Section 3.3.).

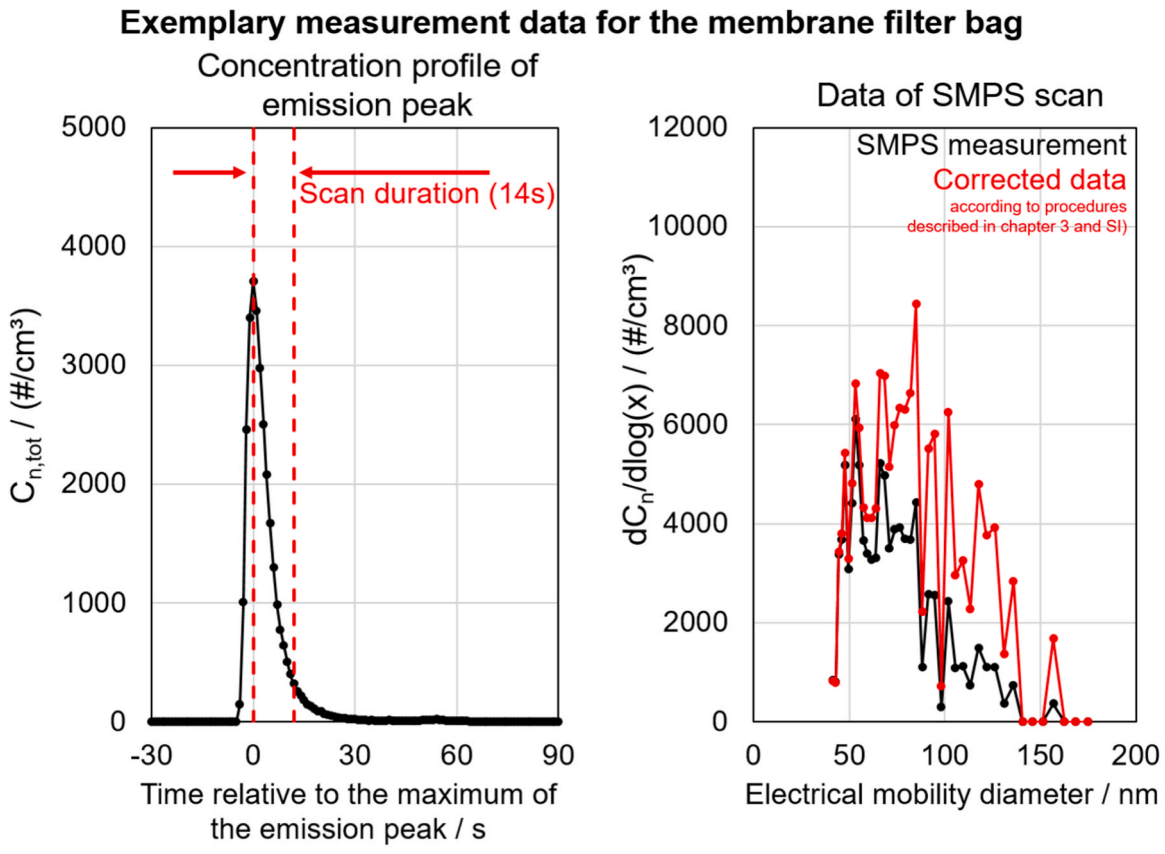

Fig. 8. Measured particle concentration profile (left) and particle size distribution (right) of the total concentration for a single SMPS scan for the membrane filter bag.

3.3. Determination of the particle size distribution for the membrane filter bag from individual scans

The emission penetrating the membrane filter bag has a very fast decay and only occurs over a time duration of approx. 15 – 20 s. The effect of this fast decay is clearly visible in the measured particle size distribution of the SMPS scan as shown in Fig. 8. In addition to the concentration decay, an additional correction with lower impact was performed based on the residence time behavior within the SMPS system (broadening of the sharp peak in total concentration, mainly due to the residence time distribution in the aerosol neutralizer). The corresponding procedure can be found in the supplementary information (figure SI 8).

For the membrane medium, the quick concentration decay and the overall low level of total number concentration allow only for very short scan durations that are below the recommended scan times for a full-range scan. Thus, the scan range has to be constricted to a subrange, where particles are to be expected (range can be derived from the measurements with constant classifier voltage), and the scan start has to be precisely timed with the emission peak. In addition to the unfavorable scan duration, the concentration decay greatly impacts the detected concentration in the corresponding size fractions. Fig. 8 clearly demonstrates that only a single scan is possible for the membrane filter medium. Consecutive scans yield zero (or close to zero) concentrations among all size fractions.

Fig. 9 shows the results of the corrected density distributions $q_0(x)$ for all performed SMPS scans for the membrane filter bag.

The fast concentration decay makes scanning of a wider distribution impossible, as concentrations decline so quickly that the concentrations in upper size classes, which are detected at the end of the scan would be negligible. Thus, obtaining a complete particle size distribution is not possible during a single individual scan. Contrary to the constant scanning settings applied for the needle-felt filter bags, for the membrane medium the range of size fractions for a single scan was changed over the individual measurements of consecutive regeneration events. Here, different objectives were aimed for during the individual scans. While measurement 1 and 2 of Fig. 9 should give a general size range of the majority of the distribution around the peak size, e.g. measurement 5 and measurement 6 are complimentary measurements where the upper and lower end of the distribution was scanned.

Combining the individual scan results (Fig. 9) enables the reconstruction of the full PSD from individual measurements. This can be achieved by using several conditions of the normalized density distribution.

One general condition of calculated density distributions (Eq. 3.1) is the area below the distribution $q_0(x)$ within the lower and upper particle size limits x_{min} and x_{max} which amounts to unity (Eq. 3.2).

$$\int_{x_{min}}^{x_{max}} q_0(x)dx = 1 \tag{3.2}$$

However, if a measurement does not cover the complete range of the emitted particle size spectrum, x_{min} and x_{max} are the borders of the measured range instead of the total size range of the complete size distribution. Thus, the distribution is normalized by the total concentration between size class x_{min} and x_{max} rather than the real total concentration of the aerosol. To correctly combine a number of i individual measurements into one global and complete normalized size distribution $\overline{q_0}(x)$, the measured subdistributions $q_{0,i}(x)$ have to be scaled down by the fraction f_i of particles covered by the individual measurement, so that the integral of $q_{0,i}(x)\cdot f_i$ over the measured size range yields less than unity.

Unfortunately, the scaling factor f_i cannot be derived from a single individual measurement i. Instead, for the determination of fi and the average size distribution two conditions have to be met.

The integral of overlapping regions (e.g. area between x_1 and x_2) of size distributions have to yield the same area according to Eq. 3.3.

$$f_1 \bullet \int_{x_1}^{x_2} q_{0,1}(x)dx = f_2 \bullet \int_{x_1}^{x_2} q_{0,2}(x)dx = \ldots = f_n \bullet \int_{x_1}^{x_2} q_{0,n}(x)dx \tag{3.3}$$

This enables averaging of the density distribution within overlapping regions of the corresponding measurements (Eq. 3.4). If only a single distribution scan detected particles in specific size classes (e.g. lower end of size distribution from measurement 5), averaging is not possible and the PSD has to be taken at face value (while still applying the previously determined scaling factor f_5).

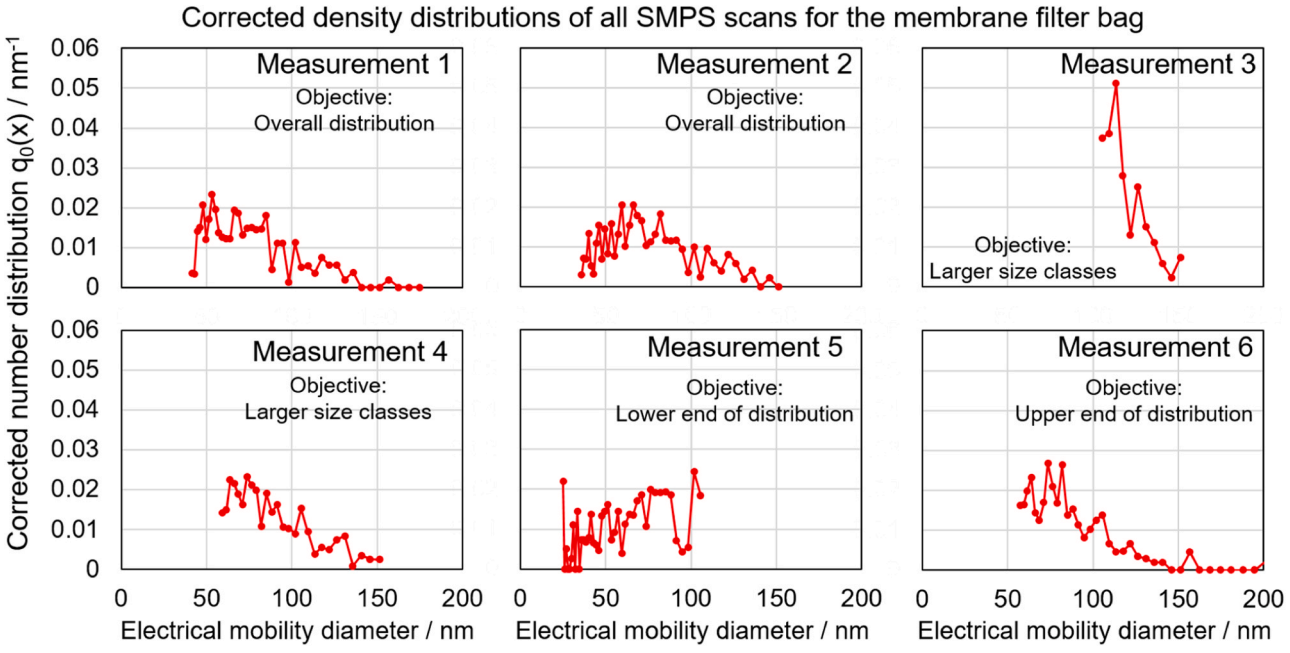

Fig. 9. Corrected density distributions for all performed SMPS scans for the membrane filter bag (measurements are in chronological order, yet no trend may be derived between the individual scans due to limited data availability).

$$\overline{q_0}(x) = \frac{1}{n}\sum_{i=1}^{n} q_{0,i}(x) \text{ for } C_{n,tot,i} > 0 \quad (3.4)$$

The final combined size distribution from all measurements ($\overline{q_0}(x)$) has to be normalized applying a factor f* so that the integral over $\overline{q_0}(x)$ yields unity according to Eq. 3.5.

$$f^* \bullet \int_{x_{min}}^{x_{max}} \overline{q_0}(x)dx = 1 \quad (3.5)$$

Fig. 10 shows the overlap of the individual measurements after scaling the corresponding distributions and the final average density distribution $\overline{q_0}(x)$. Due to the low number of counting events, an additional moving average over 5 values was calculated to smoothen the curve.

Summarizing, the determination of the emission PSD for the membrane filter bag required the combination of measurements of multiple scans, as the complete PSD cannot be obtained during a single measurement due to the fast concentration decay. Thus, during the complete scope of the field measurements, only one complete size distribution was derived, resulting from the merging process of all measurements from individual regeneration events.

4. Results

4.1. Particle size distributions of the emissions for filter bags made of different filter media

Although the transient emission behavior posed several challenges, it was possible to determine the particle size distributions of the particulate emission penetrating the filter elements after regeneration based on the procedures described in chapter 3. Fig. 11 gives a comparison of the detected number-based density distributions of the particle emission for all investigated filter bags made from the different filter media.

Note that due to the different decay behavior of the particle emission for the corresponding filter media, the procedures for the determination of PSDs had to be adapted. While the newly installed needle-felt filter bags allowed for averaging of several consecutive scans (minimum of 13 scans for each individual cycle) within a filtration cycle, only one (or at the most two) suitable scans could be obtained during each individual filtration cycle for the aged needle felt filter bag. The average distribution for the aged needle-felt filter bag shown in Fig. 11 is the result of a total of 7 individual scans (first scan of 7 measurements only). For the membrane filter bag, almost the same number of scans was required to generate a single suitable size distribution by combination of the corresponding PSDs from the individual measurements (Section 3.3).

Overall, the distributions for the two needle-felt filter bags have slightly different modes, whereby the aged needle-felt filter bag has a higher mode at 110 – 120 nm so that the fraction of smaller particles (e.g. UFP below 100 nm) relative to the total size distribution is lower compared to the newly installed needle-felt with a mode of 100 – 110 nm. Particles were detected ranging from approx. 40 nm up to 250 nm, which is only barely ranging into the detectable size range of scattered light-based aerosol spectrometers. Exemplary data from the scattered-light based emission measurements can be found in the supplementary information. Regarding the filter bag made of membrane filter medium, the mode is located at approx. 70–80 nm and (almost) no particles larger than 170 nm penetrate to the clean gas side. The lower end of the size distribution for the membrane is approx. 20 nm, but was only part of a single scan and is not concisely reflected in the PSD. Even though the mode of the membrane filter bag is smaller so that the fraction of smaller particles relative to the entire distribution is larger, the overall emission level is magnitudes lower compared to the other filter elements.

4.2. Average particle number concentrations of the particle emission for the corresponding filter bags made of different filter media

In addition to the size distribution, the average emitted particle concentration has to be taken into account for a complete evaluation of the emission and the separation efficiency of the pulse-jet cleaned filter. Total concentrations were monitored continuously for a multitude of filtration cycles for each filter medium. By calculating the integral of the emission peak related to the duration of a complete filtration cycle (80 min), the average concentration of particle emission can be calculated. In cases, where the emission peak was not measured until reaching zero emission level, the total emission of the corresponding cycle was estimated based on the relative concentration decay up to the end of the measurement. Note that this was most often the case for the newly installed needle-felt filter bag due to the slower decay and is a correction towards higher emissions. Particle losses due to the measurement setup (Section 2.2.) were considered in the concentrations stated in Fig. 12.

Even after filter regeneration, the maximum concentrations of the emission peaks (compare Fig. 4 and Fig. 5) correspond to filter separation efficiencies larger than 99%. Due to the zero emission level after the concentration decay, the average concentrations for a complete filtration cycle are orders of magnitude lower. Three distinct levels can be identified, with the membrane filter element having the lowest emissions. Compared to the membrane filter bag, the emission of the needle-felt filter bags is one order of magnitude higher for the aged needle-felt filter bag and two orders of magnitudes higher for the newly-installed needle-felt filter bag. This reflects the positive effect of filter aging on filter operation as long as the differential pressure of the filter medium

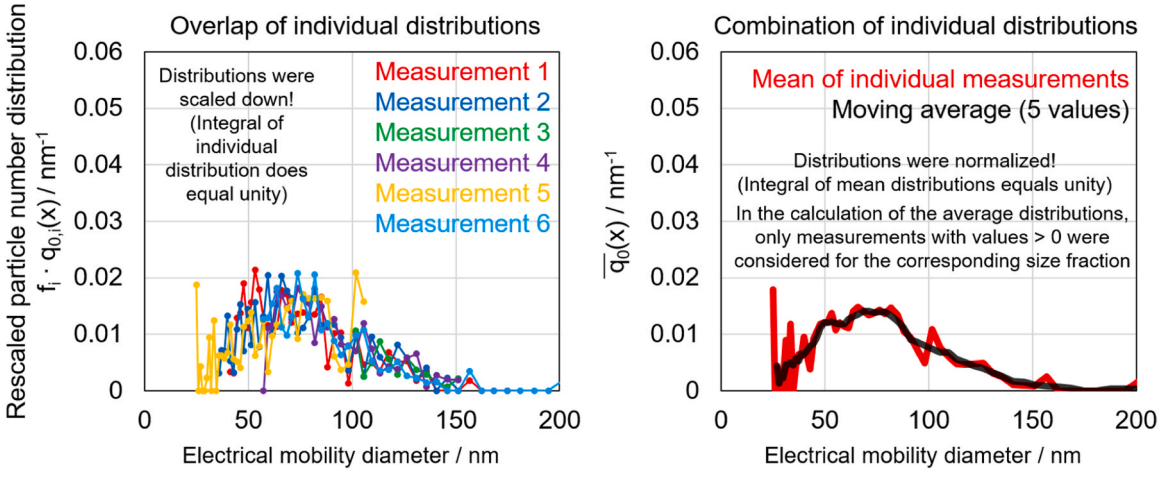

Fig. 10. Corrected density distributions for all performed SMPS scans for the membrane filter bag (compare Fig. 9 - measurements are in chronological order).

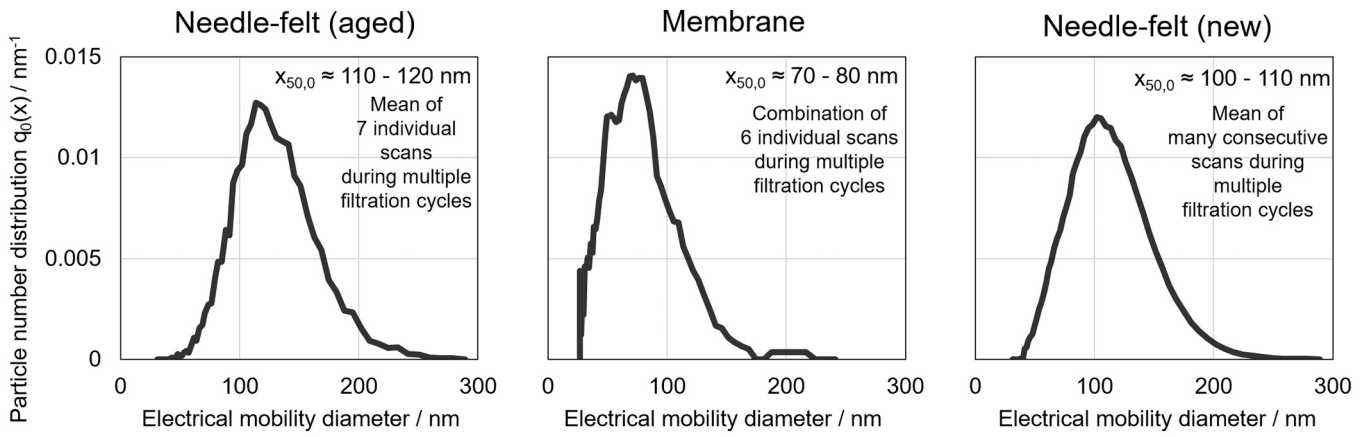

Fig. 11. Corrected density distributions of the particle emission for all three investigated filter elements (result of the average distributions from the corresponding scans during several filtration cycles).

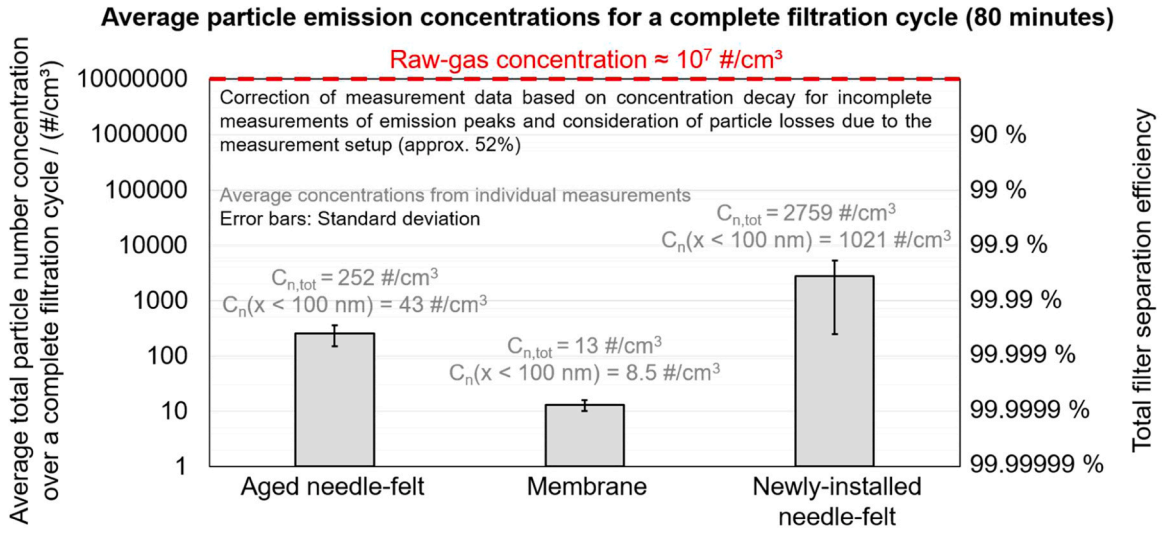

Fig. 12. Average particle emission concentrations for all three investigated filter bags made from different filter media.

remains manageable and no clogging/unstable filter operation occurs (Cirqueira et al., 2019, Saleem and Krammer, 2012). The behavior corresponds to the general observations found in literature in a filter test rig (Bächler et al., 2019) and could be validated in the field measurements. Summarizing, all investigated filter bags demonstrate high separation efficiencies and the potential for pulse-jet cleaned filters as high efficiency gas cleaning technology for biomass combustion processes. At present, electrostatic precipitators are often applied as an alternative technology which may not always reach the same efficiencies compared to fabric filters (Bürger and Riebel, 2022). The membrane filter element and the aged needle-felt filter element demonstrated average particle number concentrations even below the typical ambient background level (≈ 6000 – 10000 #/cm^3 based on on-site measurements during the field measurement campaign).

5. Summary and Outlook

The nanoparticle emission of a municipal biomass incineration plant equipped with pulse-jet cleaned filters was measured applying a complex measurement setup consisting of a sample conditioning system (heating, aerosol drying, cooling), an SMPS system and an additional CPC. Simultaneous monitoring of total concentration with a CPC and size-resolved concentration with the SMPS system enabled the determination of particle-size distributions from transient particle emission peaks after elaborate post-processing of measurement data (compare chapter 3).

The average particle emission of the membrane filter element is very low at approx. 13 #/cm^3 corresponding to a number-based filter efficiency larger than 99.999 %. The newly installed needle-felt filter bag showed emissions approx. two orders of magnitudes higher at 2759 #/cm^3. Filter aging may substantially lower emissions, as the aged needle-felt filter bag represents an intermediate emission level at 252 #/cm^3. While the needle-felt filter elements emitted a similar size distribution (mode at 100–120 nm), the membrane filter bag showed a smaller mode at 70–80 nm.

The results demonstrate the capabilities of pulse-jet cleaned filters as waste-gas cleaning technology for incineration plants. Especially the filter bag made of membrane filter medium and with sealed seams reduces emissions to levels way below ambient concentrations.

Measurement on a number basis employing SMPS and CPC technology show the drawbacks of conventional mass-based dust monitoring. On a number basis, a separation efficiency of 99% still corresponds to high nanoparticle emissions in the region of 100 000 #/cm^3 while the mass-based emission may be below the detection limit of periodic emission inspections.

Regarding further research, comparison of the results to other gas treatment technologies typical for biomass incineration plants (e.g. electrostatic precipitators) would be of interest. Additionally, long-term

stability of the membrane medium is of further interest to ensure ecological and economical gas cleaning. The conclusions drawn from the measurement methodology from the field measurements may also be transferred to the lab and included in filter testing for surface filter media in order to correctly characterize the nanoparticle emission of surface filter media for pulse-jet cleaned filters.

Declaration of Competing Interest

The authors declare that they have no known competing financial interests or personal relationships that could have appeared to influence the work reported in this paper.

Acknowledgements

We acknowledge the collaboration of Kraftwärmeanlagen GmbH (Bietigheim-Bissingen) and Rudolf Renner for the support and permission to perform the measurements at the municipal biomass incineration plant.

conflict of interest

The authors declare no conflict of interest.

Appendix A. Supporting information

Supplementary data associated with this article can be found in the online version at doi:10.1016/j.psep.2024.02.013.

References

Bächler, P., Löschner, V., Meyer, J., Dittler, A., 2022b. Process integrated monitoring of spatially resolved particle emissions of a baghouse filter using a network of low-cost PM-sensors. Process Saf. Environ. Prot. 160, 411–423. https://doi.org/10.1016/j.psep.2022.02.005.

Bächler, P., Meyer, J., Dittler, A., 2019. Characterization of the emission behavior of pulse-jet cleaned filters using a low-cost particulate matter sensor. Gefahrst. – Reinhalt. der Luft. 79 (11-12), 443–450. https://doi.org/10.37544/0949-8036-2019-11-12-49.

Bächler, P., Meyer, J., Dittler, A., 2022a. Measurement of transient nanoparticle emissions of pulse-jet cleaned filters applying an engine exhaust particle sizer. Aerosol Sci. Technol. 56 (4), 394–402. https://doi.org/10.1080/02786826.2022.2027335.

Bächler, P., Meyer, J., Dittler, A., 2023a. Spatially Resolved Online Leak Detection in a Baghouse Filter Applying Low-Cost PM-Sensors. Chem. Ing. Tech. 95 (1-2), 178–188. https://doi.org/10.1002/cite.202200116.

Bächler, P., Meyer, J., Dittler, A., 2023b. Operating Behavior of Pulse Jet-Cleaned Filters Regarding Energy Demand and Particle Emissions – Part 1: Experimental Parameter Study. Chem. Eng. Technol. 46 (8), 1689–1697. https://doi.org/10.1002/ceat.202300080.

Bächler, P., Szabadi, J., Meyer, J., Dittler, A., 2020. Simultaneous measurement of spatially resolved particle emissions in a pilot plant scale baghouse filter applying distributed low-cost particulate matter sensors. J. Aerosol Sci. Vol. 150, 105644 https://doi.org/10.37544/0949-8036-2019-11-12-49.

Bach, B., Schmidt, E., 2007. Influence of leaks in surface filters on particulate emissions. J. Hazard. Mater. 143 (3), 673–676. https://doi.org/10.1016/j.jhazmat.2007.01.093.

Bari, M., A., Baumbach, G., Kuch, G., Scheffknecht, G., 2010. Temporal variation and impact of wood smoke pollution on a residential area in southern Germany. Atmos. Environ. 44 (31), 3823–3832. https://doi.org/10.1016/j.atmosenv.2010.06.031.

Binnig, J., Meyer, J., Kasper, G., 2009. Origin and mechanisms of dust emission from pulse-jet cleaning filter media. Powder Technol. 189 (1), 108–114. https://doi.org/10.1016/j.powtec.2008.06.012.

Bürger, P., Riebel, U., 2022. Feasibility of high-temperature electrostatic precipitation for the removal of nanoparticles: A case study on iron oxide separation at up to 800 °C. J. Electrost. 120, 103754 https://doi.org/10.1016/j.elstat.2022.103754.

Cirqueira, S.S.R., Tanabe, E.H., Aguiar, M.L., 2017. Evaluation of operating conditions during the pulse jet cleaning filtration using different surface treated fibrous filters. Process Saf. Environ. Prot. 105, 69–78. https://doi.org/10.1016/j.psep.2016.10.010.

Cirqueira, S.S.R., Tanabe, E.H., Aguiar, M.L., 2019. Experimental investigation of particle deposition in filter media during filtration cycles with regeneration by pulse jet cleaning. Process Saf. Environ. Prot. 127, 288–298. https://doi.org/10.1016/j.psep.2019.05.013.

Ergüdenler, A., Tang, W., Brereton, C., M., H., Jim Lim, C., Grace, J., R., Gennrich, T., J., 1997. Performance of high-temperature fabric filters under gasification and combustion conditions. Sep. Purif. Technol. 11, 1–16. https://doi.org/10.1016/S1383-5866(96)01002-7.

Eriksson, O., Finnveden, G., Ekvall, T., Björklund, A., 2007. Life cycle assessment of fuels for district heating: A comparison of waste incineration, biomass- and natural gas combustion. Energy Policy 2, 1346–1362. https://doi.org/10.1016/j.enpol.2006.04.005.

European Commission, Proposal for a DIRECTIVE OF THE EUROPEAN PARLIAMENT AND OF THE COUNCIL on ambient air quality and cleaner air for Europe (recast). ⟨https://environment.ec.europa.eu/publications/revision-eu-ambient-air-quality-legislation_en⟩ (accessed 10 January 2024).

German National Academy of Sciences Leopoldina (2019). Clean air. Nitrogen oxides and particulate matter in ambient air: Basic principles and recommendations. Halle (Saale).

Daginnus, K., Marty, T., Trotta, N.V., Brinkmann, T., Whitfield, A., Roudier, S., 2023. European Commission Joint Research Centre Best available techniques (BAT) reference document for common waste gas management and treatment systems in the chemical sector Industrial Emissions Directive 2010/75/EU (Integrated pollution prevention and control). Publications Office of the European Union. https://doi.org/10.2760/220326.

Helsper, C., Fissan, H., J., Muggli, J., Scheidweiler, A., 1980. Particle number distributions of aerosols from test fires. J. Aerosol Sci. 11 (5-6), 439–446. https://doi.org/10.1016/0021-8502(80)90116-0.

Hermansson, S., Lind, F., Thunman, H., 2011. On-line monitoring of fuel moisture content in biomass-fired furnaces by measuring relative humidity of the flue gases. Chem. Eng. Res. Des. 89 (11), 2470–2476. https://doi.org/10.1016/j.cherd.2011.03.018.

Hueglin, C., Gaegauf, S., Künzel, S., Burtscher, H., 1997. Characterization of wood combustion particles: Morphology, Mobility, and Photoelectric activity. Environ. Sci. Technol. 31 (12), 3439–3447. https://doi.org/10.1021/es970139i.

Johansson, L., S., Tullin, C., Leckner, B., Sjövall, P., 2003. Particle emissions from biomass combustion in small combustors. Biomass-.-. Bioenergy 25 (4), 435–446. https://doi.org/10.1016/S0961-9534(03)00036-9.

Kaminski, H., Kuhlbusch, T., A., J., Rath, S., Götz, U., Sprenger, M., Wels, D., Polloczek, J., Bachmann, V., Dziurowitz, N., Kiesling, H.-J., Schwiegelshohn, A., Monz, C., Dahmann, D., Asbach, C., 2013. Comparability of mobility particle sizers and diffusion chargers. J. Aerosol Sci. 57 (2013), 156–178. https://doi.org/10.1016/j.jaerosci.2012.10.008.

Khirouni, N., Charvet, A., Thomas, D., Bémer, D., 2020. Regeneration of dust filters challenged with metallic nanoparticles: Influence of atmospheric aging. Process Saf. Environ. Prot. 138 (2020), 1–8. https://doi.org/10.1016/j.psep.2020.02.040.

Klingel, R., Löffler, F., 1983. Dust collection and cleaning efficiency of a pulse-jet fabric. Filtr. Sep. 20 (3), 205–208.

Kurtz, O., Meyer, J., Kasper, G., 2017. The contribution of small leaks in a baghouse filter to dust emission in the $PM_{2.5}$ range – A system approach. Particuology 30, 40–52. https://doi.org/10.1016/j.partic.2016.08.001.

Lacerda, C., R., Bächler, P., Schwarz, A., D., Sartim, R., Aguiar, M., L., Dittler, A., 2022. Impact of Seams on the Operating Behavior of Surface Filters Regarding Particle Emissions. Chem. Eng. Technol. 45 (7), 1354–1362. https://doi.org/10.1002/ceat.202200132.

Leith, D., Ellenbecker, M., J., 1980. Theory for pressure drop in a pulse-jet cleaned filter (1967). Atmos. Environ. 14 (7), 845–852. https://doi.org/10.1016/0004-6981(80)90141-9.

Li, J., Wu, Q., Huang, Y., Sun, Z., Li, J., Wu, D., 2022. Particulate matters filtration by a filter medium with pin holes: modeling and experimental verification. Process Saf. Environ. Prot. 158, 282–290. https://doi.org/10.1016/j.psep.2021.12.012.

Mishra, S., Sundaram, B., 2023. Fate, transport, and toxicity of nanoparticles: An emerging pollutant on biotic factors. Process Saf. Environ. Prot. 174, 595–607. https://doi.org/10.1016/j.psep.2023.04.037.

Monsberger, C., Maggauer, K., Fina, B., Suna, D., Fuchs, C., Leitner, B., 2023. Profitability of biomass-based district heating considering different technology combinations and building flexibility. Renew. Sustain. Energy Transit. 4, 100062 https://doi.org/10.1016/j.rset.2023.100062.

Obaidullah, M., Bram, S., Verma, V., K., de Ruyck, J., 2012. A review on particle emissions from small scale biomass combustion. Int. J. Renew. Energy Res. 2 (1), 147–159.

Ohlwein, S., Kappeler, R., Joss, M., K., Künzli, N., Hoffmann, B., 2019. Health effects of ultrafine particles: a systematic literature review update of epidemiological evidence. Int. J. Public Health 64, 547–559. https://doi.org/10.1007/s00038-019-01202-7.

Rogoziński, T., 2018. Pilot-scale study on the influence of wood dust type on pressure drop during filtration in a pulse-jet baghouse. Process Saf. Environ. Prot. 119 (2018), 58–64. https://doi.org/10.1016/j.psep.2018.07.016.

Saleem, M., Krammer, G., 2012. On the Stability of Pulse-Jet Regenerated-Bag Filter Operation. Chem. Eng. Technol. 35 (5), 877–884. https://doi.org/10.1002/ceat.201100516.

Saleem, M., Krammer, G., Khan, R.U., Tahir, M., S., 2012. Influence of operating parameters on cake formation in pilot scale pulse-jet bag filter. Powder Technol. 224, 28–35. https://doi.org/10.1016/j.powtec.2012.02.016.

Schiller, S., Schmid, H., J., 2015. Highly efficient filtration of ultrafine dust in baghouse filters using precoat materials. Powder Technol. 279, 96–105. https://doi.org/10.1016/j.powtec.2015.03.048.

Schiller, S., Schmid, H., J., 2014. Ultrafine Dust Filtration Using Precoat Materials Considering the Influence of Filter Media. Chem. Eng. Technol. 37 (6), 1009–1020. https://doi.org/10.1002/ceat.201300856.

Schiller, S., Schmid, H., J., 2013. Highly Efficient Fine Dust Deposition from Small-Scale Heating Systems with a Baghouse Filter. Chem. Ing. Tech. 85 (8), 1324–1328. https://doi.org/10.1002/cite.201200114.

Schmidt, E., (1998). Abscheidung von Partikeln aus Gasen mit Oberflächenfiltern, Fortschritt-Berichte der VDI-Zeitschriften, Reihe 3 (546). Düsseldorf: VDI Verlag.

Schott, F., Baumbach, G., Straub, D., Thorwarth, H., Vogt, U., 2022. Novel metal mesh filter equipped with pulse-jet regeneration for small-scale biomass boilers. Biomass-.-. Bioenergy 163, 106520. https://doi.org/10.1016/j.biombioe.2022.106520.

Simon, X., Bémer, D., Chazelet, S., Thomas, D., Régnier, R., 2010. Consequences of high transitory airflows generated by segmented pulse-jet cleaning of dust collector filter bags. Powder Technol. 201 (1), 37–48. https://doi.org/10.1016/j.powtec.2010.02.036.

Simon, X., Bémer, D., Chazelet, S., Thomas, D., 2014. Downstream particle puffs emitted during pulse-jet cleaning of a baghouse wood dust collector: Influence of operating conditions and filter surface treatment. Powder Technol. 261, 61–70. https://doi.org/10.1016/j.powtec.2014.04.028.

Soares, J., González Ortiz, A., Gsella, A., Horálek, J., Plass, D. & Kienzler, S. (2022). Health risk assessment of air pollution and the impact of the new WHO guidelines (Eionet Report – ETC HE 2022/10). European Topic Centre on Human Health and the Environment ⟨https://www.eionet.europa.eu/etcs/etc-he/products/etc-he-products/etc-he-reports/etc-he-report-2022-10-health-risk-assessment-of-air-pollution-and-the-impact-of-the-new-who-guidelines⟩; accessed 10. January 2024).

Soltero, V., M., Quirosa, G., Rodríguez, D., Ortiz, C., Chacartegui, R., 2023. A profitability index for rural biomass district heating systems evaluation. Energy 282, 128395. https://doi.org/10.1016/j.energy.2023.128395.

Steiner, D., Lanzerstorfer, C., 2023. Particulate emissions from biomass power plants: a practical review and measurement uncertainty issues. Clean Technol. Environ. Policy. https://doi.org/10.1007/s10098-023-02645-6.

Thieringer, J., R., D., Szabadi, J., Meyer, J., Dittler, A., 2022. Impact of Residential Real-World Wood Stove Operation on Air Quality concerning PM2.5 Immission. Processes 10 (3), 545. https://doi.org/10.3390/pr10030545.

Tsai, C.-J., Tsai, M.-L., Lu, H.-C., 2000. Effect of Filtration Velocity and Filtration Pressure Drop on the Bag-Cleaning Performance of a Pulse-Jet Baghouse. Sep. Sci. Technol. 35 (2), 211–226. https://doi.org/10.1081/SS-100100152.

WHO global air quality guidelines. Particulate matter (PM2.5 and PM10), ozone, nitrogen dioxide, sulfur dioxide and carbon monoxide. Geneva: World Health Organization 2021.

Xie, Q., Yuan, H., Song, L., Zhang, Y., 2007. Experimental studies on time-dependent size distributions of smoke particles of standard test fires. Build. Environ. 42, 640–646. https://doi.org/10.1016/j.buildenv.2005.10.014.

Zhang, Q., 2021. Online Particle Measurement in Clean Gas at the Beginning of Cake-forming Dust Separation with Needled Felts in the Gas Cleaning. Chem. Eng. Technol. 94 (4), 572–584. https://doi.org/10.1002/cite.202100053.

Zhang, R., Xu, G., Li, B., Wang, Z., Gao, J., Li, J., Sun, Y., Xu, G., 2023. Analysis of the pollution emission system of large-scale combustion of biomass briquette fuel in China. Process Saf. Environ. Prot. 169, 928–936. https://doi.org/10.1016/j.psep.2022.11.088.